INTERFACE

rsif.royalsocietypublishing.org

Research

Cite this article: Bluman JE, Sridhar MK, Kang C-k. 2018 Chordwise wing flexibility may passively stabilize hovering insects. *J. R. Soc. Interface* **15**: 20180409.
http://dx.doi.org/10.1098/rsif.2018.0409

Received: 4 June 2018
Accepted: 7 September 2018

Subject Category:
Life Sciences–Engineering interface

Subject Areas:
biomechanics, biomimetics

Keywords:
insect flight, flapping wing stability, fluid–structure–dynamic interaction

Author for correspondence:
Chang-kwon Kang
e-mail: ck0025@uah.edu

†Present address: Department of Civil and Mechanical Engineering, United States Military Academy, West Point, NY 10996, USA.

THE ROYAL SOCIETY PUBLISHING

Chordwise wing flexibility may passively stabilize hovering insects

James E. Bluman†, Madhu K. Sridhar and Chang-kwon Kang

Department of Mechanical and Aerospace Engineering, University of Alabama in Huntsville, 301 Sparkman Drive, Huntsville, AL 35899, USA

C-KK, 0000-0001-9353-4519

Insect wings are flexible, and the dynamically deforming wing shape influences the resulting aerodynamics and power consumption. However, the influence of wing flexibility on the flight dynamics of insects is unknown. Most stability studies in the literature consider rigid wings and conclude that the hover equilibrium condition is unstable. The rigid wings possess an unstable oscillatory mode mainly due to their pitch sensitivity to horizontal velocity perturbations. Here, we show that a flapping wing flyer with flexible wings exhibits stable hover equilibria. The free-flight insect flight dynamics are simulated at the fruit fly scale in the longitudinal plane. The chordwise wing flexibility is modelled as a linear beam. The two-dimensional Navier–Stokes equations are solved in a tight fluid–structure integration scheme. For a range of wing flexibilities similar to live insects, all eigenvalues of the system matrix about the hover equilibrium have negative real parts. Flexible wings appear to stabilize the unstable mode by passively deforming their wing shape in the presence of perturbations, generating significantly more horizontal velocity damping and pitch rate damping. These results suggest that insects may passively stabilize their hover flight via wing flexibility, which can inform designs of synthetic flapping wing robots.

1. Introduction

Small flapping wing flyers such as insects are truly remarkable creatures. Across the taxonomic class *Insecta*, they exhibit an enviable slate of characteristics that includes highly agile flight, the ability to perform long migrations and the ability to carry excess loads approaching their own weight. They clearly possess the propulsion mechanisms, energy stores and control systems sufficient to achieve these flying feats, as well as the sensing and processing abilities to command them. These characteristics make insects a natural source of biomimicry for scientists and engineers attempting to design and construct artificial flapping wing micro-air vehicles (FWMAVs).

Many flying insects can hover. This energetically demanding flight mode is realized by using low Reynolds number (Re) unsteady lift enhancement mechanisms [1]. The well-known mechanisms of delayed stall, rotational lift, added mass forces and wake-capture characterize the hovering flight of insects.

An open research question in the flight of insects and FWMAV is the stability of flapping wings. To maintain its position in hover, an insect not only generates sufficient aerodynamic forces to offset its weight and drag, it also must hold its position in an equilibrium condition. However, the hovering equilibria are reported to be unstable for flapping wing flyers [2,3]. The most common method of describing the stability of insects is by presenting the eigenvalues λ_i of the linearized system matrix [2,4,5]. Also known as open-loop poles, the literature reports on hover eigenvalues for a number of insect families, including drone flies, fruit flies, bumblebees, hawkmoths and hover flies. The studies include several different aerodynamic modelling techniques. Yet, they overwhelmingly share the same natural modes of motion, plotted on the complex plane in figure 1. The fast and slow subsidence modes are stable. The complex pair of

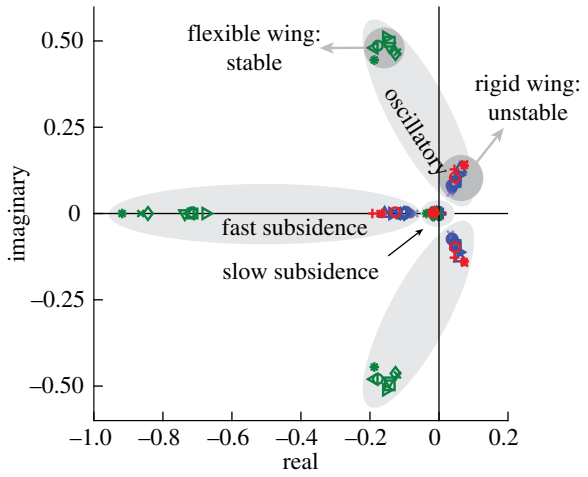

Figure 1. Open-loop poles for multiple insect species from studies that assume rigid wings (times: hover fly [6]; open circles: dronefly [6,7]; plus: bumblebee [8]). Simulations [9] using a Navier–Stokes aerodynamic model and measured fruit fly pitch angles [10] with different axes of rotation considered are blue. Flexible wings with different values of wing stiffness are green. The open-loop poles are normalized with respect to each insect's flapping period and therefore have units of (flapping period)$^{-1}$.

eigenvalues representing the oscillatory mode is located on the right half of the complex plane, indicating that the system is unstable. In spite of the different insects studied and the different aerodynamic models employed, these reports share a single unifying simplification—the wings are assumed to be rigid [2–5,11–17].

Flying insects have flexible wings [18–22], which results from the complicated structure of thicker veins and interstitial resilin. Recent investigations have shown that wing flexibility reduces the power requirement by lowering torque and drag penalties [23] and enhances the load lifting capacity of bumblebees [18] by altering the unsteady aerodynamics around the flapping wings [24].

The objective of this study was to test the hypothesis that the structural flexibility of flapping wings produces a stabilizing influence on the insect while in hover. We use the data from a computational experiment [9] to calculate the stability derivatives of a freely flying fruit fly scale flapping model with flexible wings while in hover. Our results show that the real part of all system eigenvalues associated with flexible wings are negative (figure 1), suggesting that the hover equilibrium of flexible flapping wings is linearly stable. A flexible wing adjusts its structural dynamic response under a perturbation, a feature not available to a rigid wing. The enhanced damping associated with wing flexibility yields a stable hover equilibrium across a range of different values of wing stiffness.

2. Models and methods

The flight dynamics of a flapping flyer with flexible wings is governed by the complex three-way coupling of aerodynamics, structural dynamics and flight dynamics [4,11]: the aerodynamic loads, governed by the nonlinear unsteady viscous Navier–Stokes equations, depend on the wing deformation, which, at the same time, depends on the aerodynamic loads. Additionally, the resulting aerodynamic loading affects the body dynamics, which, in turn, changes the wing aerodynamics and wing shapes. Because of this challenge, most theoretical and numerical studies in the literature [2,4,11] assume rigid wings, simulate flight in the longitudinal plane and conclude that the hover equilibrium is unstable.

In this study, we analyse the numerical data from an insect flight simulator that is fully coupled to the unsteady aerodynamics and flexible wing dynamics [9]. The detailed discussion of the governing equations, computational methodology, computational set-up and validation studies are reported in our previous work [9]. A description of the governing equations is summarized in appendix A for completeness.

2.1. Flapping kinematics and passive pitch motion

We impose a bioinspired flapping motion ζ [25] on the leading edge of a wing as follows:

$$\zeta(t) = \frac{Z}{\sin^{-1}K}\sin^{-1}(K\cos[2\pi ft]) + \zeta_\varphi, \tag{2.1}$$

where f is the flapping frequency, t is time and Z is the flapping amplitude (figure 2*a*). The flapping motion can be biased fore and aft of the body y-axis by a positive or negative flapping offset angle ζ_φ. We set $K = 0.01$, which keeps the flapping motion nearly sinusoidal. The reference velocity is the maximum translational velocity of the second moment of wing area r_2, $U = 2\pi f r_2 Z$.

We select the flapping amplitude Z, the stroke plane angle β and the flapping offset angle ζ_φ as control inputs that place the insect in equilibrium based on methods used by previous researchers [14,26]. These methods were altered to accommodate the influence of wing flexibility in our previous work [9].

The key feature in this study is that the wing pitch angle is not prescribed. Rather, the instantaneous wing pitch α_{flex} results from the dynamic balance between the wing's inertia, elastic restoring force and aerodynamic forces. Furthermore, body motion is superimposed on the flapping motion, both of which can affect the resulting wing motion. Unlike most rigid or flexible flapping aerodynamics studies [27,28], where the insect is fixed and only resulting forces are analysed, we allow the body to respond to the instantaneous aerodynamic forces and moments. As a result, the leading edge of the wing also moves through multiple degrees of freedom, which, in turn, affects the resulting aerodynamics and fluid–structure interaction.

2.2. Fluid–structure–dynamic interaction

The aerodynamic forces and moments are calculated directly by the coupled Navier–Stokes equations and structural dynamics solvers by integrating the pressure and shear forces on the wing. It is critical to solve the Navier–Stokes equations to analyse the flapping wing aerodynamics. Insect flight is characterized by the unsteady, viscous flow features, which include wake-capture, clap and fling, dynamic stall via leading-edge vortices and rotational forces due to combined translation and rotation [29]. The equations of motion are solved to yield the body accelerations for each time step. The displacements with respect to the inertial frame are then transformed back into the computational frame and provided to the Navier–Stokes solver. The body motion is combined with the change in position and angle due to the wing motion at each time step. The computational

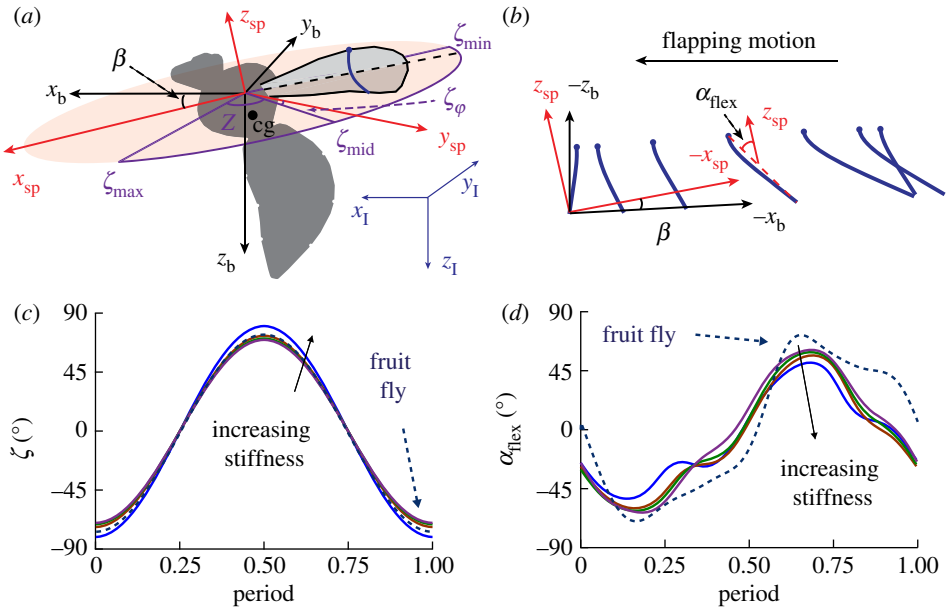

Figure 2. Schematics of the considered wing kinematics. (*a*) Fruit fly model used in the current study with pertinent reference frames. Subscripts I, b and sp refer to the inertial, body and stroke plane reference frames, respectively. (*b*) Passive pitch motion α_{flex} due to wing flexibility and body dynamics over the dorsal to ventral half-stroke for $f/f_1 = 0.41$. (*c*) Flapping and (*d*) passive pitch angles resulting from changing the wing flexibility alongside observed kinematics from a fruit fly [10].

grid is re-meshed at each time step using the radial basis function interpolation scheme [30]. Extensive validation on the flexible wing's computation framework has been previously reported [28,31,32]. Also, careful validation studies have been conducted on the open-loop stability derivatives and power required in hover for fruit fly scale rigid [33] and flexible wings [9].

To fully unveil all of the effects of insect wing flexibility, a full three-dimensional structural simulation is needed that could accurately model the interesting biological wing shapes and structures, and simultaneously resolve the nonlinear modes of the structural response with the fluid dynamic response. This is a tall order. Furthermore, such a complicated model could obscure, rather than highlight the specific influence of individual features, which would likely make determining the mechanisms for any observed benefits harder to identify. Insect wings are 10–100 times more compliant in the chordwise direction than the spanwise direction [19]. Therefore, this study considers only chordwise flexibility on a two-dimensional strip of the wing, so that the influence of the most flexible mode can be determined. The chordwise wing deformation alters the angle of attack of the wing, which significantly influences the unsteady flow dynamics and the resulting forces. We model the effects of chordwise flexibility on the resulting aerodynamics and dynamics by transforming the three-dimensional flapping wing motion about the wing root ζ to a two-dimensional plunge motion $h = \zeta r_2$ at the second moment of wing area r_2 [9]. The r_2 location accounts for the spanwise distribution of lift in an averaged sense [34,35] and is the most appropriate location to calculate the two-dimensional approximation of the three-dimensional flapping wing aerodynamics [35].

The two-dimensional unsteady, viscous flow around the chordwise flexible wing is calculated with the Navier–Stokes equations to capture all of the unsteady and viscous effects. In general, three-dimensional effects, such as spanwise flow, that seem to stabilize the leading-edge vortices (LEVs) [36], LEV–tip–vortex interaction [37], centrifugal, Coriolis and angular accelerations [38], are notable in flapping wings. However, earlier studies have shown that the effects of spanwise flow on the overall aerodynamics are less important at the fruit fly scale (considered in this study) than at higher Reynolds numbers [36,39]. Also, the characteristics of the LEVs in two dimensions for plunging motions are representative of three-dimensional flapping wings as long as the stroke-to-chord ratio is within the range of typical insects, i.e. around four to five [40–42], which we consider in this study. Finally, we showed that the minor differences in the force coefficient magnitudes between two-dimensional and three-dimensional flapping wing aerodynamics do not qualitatively affect the stability outcomes for fruit fly scale dynamics in our earlier work [33].

2.3. Frequency ratio

To determine the influence of wing flexibility on the flight performance and dynamic characteristics of the FWMAV, we adjust the Young's modulus E of the wing to determine its effects on the resultant wing and body motion. This variation is reflected in the resulting frequency ratios

$$\frac{f}{f_1} = \frac{2\pi c f}{k_1^2 h_s}\sqrt{\frac{12\rho_w}{E}}, \tag{2.2}$$

as defined in [31], where f_1 is the fundamental natural frequency of the wing in the chordwise direction based on its structural properties, c is the wing mean chord, h_s is the wing thickness and ρ_w is the wing material density. Larger values of frequency ratio correspond to more compliant wings. We hold several variables constant, while varying Young's modulus. The coefficient k_1 is based on the first natural mode of a cantilevered beam and is set to 1.875 for all of the cases in this study [31]. The frequency is fixed at $f =$ 218 Hz based on the observations of fruit flies [43]. The density of the wing is $\rho_w = 1 \times 10^3$ kg m^{-3} [31] and the thickness ratio is $h_s^* = h_s/c = 1.5 \times 10^{-3}$, where $c = 0.8$ mm based on the observations of fruit flies [44,45]. Furthermore, the wing length is $R = 2.39$ mm and $r_2 = 1.31$ mm.

We parametrically vary the stiffness from relatively stiff ($f/f_1 = 0.368$) to more compliant ($f/f_1 = 0.461$) to assess the effects of the frequency ratio on the insect hovering dynamics. We were unable to find the frequency ratio range for fruit flies in the literature; however, dragonflies are reported to fly at frequency ratios from 0.31 to 0.46 [46]. Most insects flap their wings with a flapping frequency f well below f_1 [22], and the values of f/f_1 used in the current study are also less than unity. The values of Young's modulus that correspond to these frequency ratios are listed in table 1.

2.4. Stability derivatives

We restrict our analysis to the longitudinal degrees of freedom in the pitch plane around hover equilibrium. The state vector is $\mathbf{x} = [u, w, q, {}_{\mathrm{I}}x_{\mathrm{cg}}, {}_{\mathrm{I}}z_{\mathrm{cg}}, \theta]^{\mathrm{T}}$, where u and w are the body velocities at the body centre of gravity (CG) along the x_{b} and z_{b} axes, respectively, and q is the pitch velocity about the y_{b} axis. The body CG positions ${}_{\mathrm{I}}x_{\mathrm{cg}}$ and ${}_{\mathrm{I}}z_{\mathrm{cg}}$ and the pitch attitude θ are measured in the inertial frame of reference. To find the trimmed state at hover and determine the stability derivatives, we express the nonlinear, time-varying equations of motion (appendix A) as a set of coupled, linearized equations of motion

$$\dot{\mathbf{x}} = A\mathbf{x} + B\mathbf{u}, \tag{2.3}$$

where A is the system matrix and B is the control matrix that translates changes in the applied control vector $\mathbf{u} = [Z, \beta, \zeta_\varphi]^{\mathrm{T}}$ to the changes in the rate vector $\dot{\mathbf{x}}$.

The aerodynamic forces and moments on the flapping wing flyer do not depend on the position of the body CG. As a consequence, the open-loop dynamics of a flapping wing flyer then is described by a 4×4 matrix A [2], typically written as

$$A = \begin{bmatrix} \frac{1}{m}X_u & \frac{1}{m}X_w & \frac{1}{m}X_q & g \\ \frac{1}{m}Z_u & \frac{1}{m}Z_w & \frac{1}{m}Z_q & 0 \\ \frac{1}{I_{yy}}M_u & \frac{1}{I_{yy}}M_w & \frac{1}{I_{yy}}M_q & 0 \\ 0 & 0 & 1 & 0 \end{bmatrix} \tag{2.4}$$

where the stability derivatives X_u/m, X_w/m, X_q/m, Z_u/m, Z_w/m, Z_q/m, M_u/I_{yy}, M_w/I_{yy} and M_q/I_{yy} describe the average response (over a single flapping period) of a flyer in equilibrium to a perturbation in a particular degree of freedom. X and Z are the aerodynamic forces acting on the body CG in the body frame in the x_{b} and z_{b} directions, respectively. M is the pitch moment about the body CG. The total mass is $m = 0.97$ mg, and the body inertia about the y_{b} axis is $I_{yy} = 5.1 \times 10^{-9}$ kg m^{-2}. For example, the horizontal velocity damping X_u/m is defined as

$$\frac{X_u}{m} = \frac{\Delta \dot{u}}{\delta u} = \frac{\bar{\dot{u}}(u_0 + \delta u, w_0, q_0, \theta_0) - \bar{\dot{u}}(u_0, w_0, q_0, \theta_0)}{\delta u}, \tag{2.5}$$

where the overbar indicates a cycle average of the acceleration in each degree of freedom and δu is a horizontal velocity perturbation. The hover equilibria are determined numerically [9], implying that the cycle-averaged velocities and accelerations are zero. Hover solutions are indicated with the subscript 0. The pitch rate damping M_q/I_{yy} is defined in a similar way as

$$\frac{M_q}{I_{yy}} = \frac{\bar{\dot{q}}(u_0, w_0, q_0 + \delta q, \theta_0) - \bar{\dot{q}}(u_0, w_0, q_0, \theta_0)}{\delta q}, \tag{2.6}$$

Table 1. The frequency ratio and the Young's modulus considered in this study [9]. The flapping amplitude Z and the reduced frequency k are determined to achieve hover equilibrium [9].

f/f_1	Young's modulus (N m^{-2})	Z (°)	k
0.368	7.0×10^8	75	0.235
0.390	6.5×10^8	73.5	0.239
0.414	6.0×10^8	72	0.244
0.441	5.5×10^8	71.5	0.249
0.452	5.3×10^8	70.7	0.250
0.455	5.25×10^8	70.1	0.251
0.461	5.15×10^8	69.8	0.252

where q is the body pitch rate in the body frame and δq is a pitch rate perturbation and so on. The control matrix B is obtained by perturbing each control in a similar fashion and determining its effect on the average of the rate vector.

3. Results and discussion

3.1. Passively pitching flexible flapping wings

To explain the stabilizing influence of flexible flapping wing dynamics, we systematically vary the flapping wing amplitude Z, stroke plane angle β and stroke mean angle ζ_φ (figure 2*a*), so that the insect is in a hover equilibrium with zero cycle-averaged body velocities and accelerations [9]. Once in equilibrium flight, the open-loop poles can be assessed by perturbing the dynamical system in the horizontal, vertical and pitch degrees of freedom as described in §2.4. and more in detail in our previous work [9].

The passive deformation of flexible wings (figure 2*b*) arises from the dynamic balance of the wing inertia from flapping (figure 2*c*), the aerodynamic forces and the wing's stiffness. The wing deformation results in a passive pitch angle α_{flex} (figure 2*b*,*d*) as well as significant wing camber. Previous studies [24,47] have shown that the passive pitch angles are large enough to generate enough lift to remain aloft. By contrast, most rigid wings must actively rotate to achieve similar kinematics and produce enough lift. The extent to which insects actively rotate their wings is not fully known. Although they possess the musculature to achieve pitch rotation [48], experiments have also observed tip-to-root torsion waves and other evidence that insects typically rely on passive deformation of their wings to fly [21,48]. Furthermore, being able to pitch does not necessarily imply that they always actively pitch the wing. Dynamic aspects of active and passive pitch will be considered in the future.

Figure 2*b* includes the pitch angle time history, experimentally observed for hovering fruit flies by Fry *et al*. [10]. There are some differences, which are expected due to modelling and experimental uncertainties. Nevertheless, we show in our previous work [9] that the resulting pitch motion resembles that of fruit flies and the effects of these differences on the resulting aerodynamics and flight dynamics are small: (i) we solve for the flapping amplitude and stroke plane angle to place the system in hover equilibrium. The flapping amplitude and stroke plane angle solutions are similar to those observed for fruit flies [9]. (ii) The resulting time-averaged

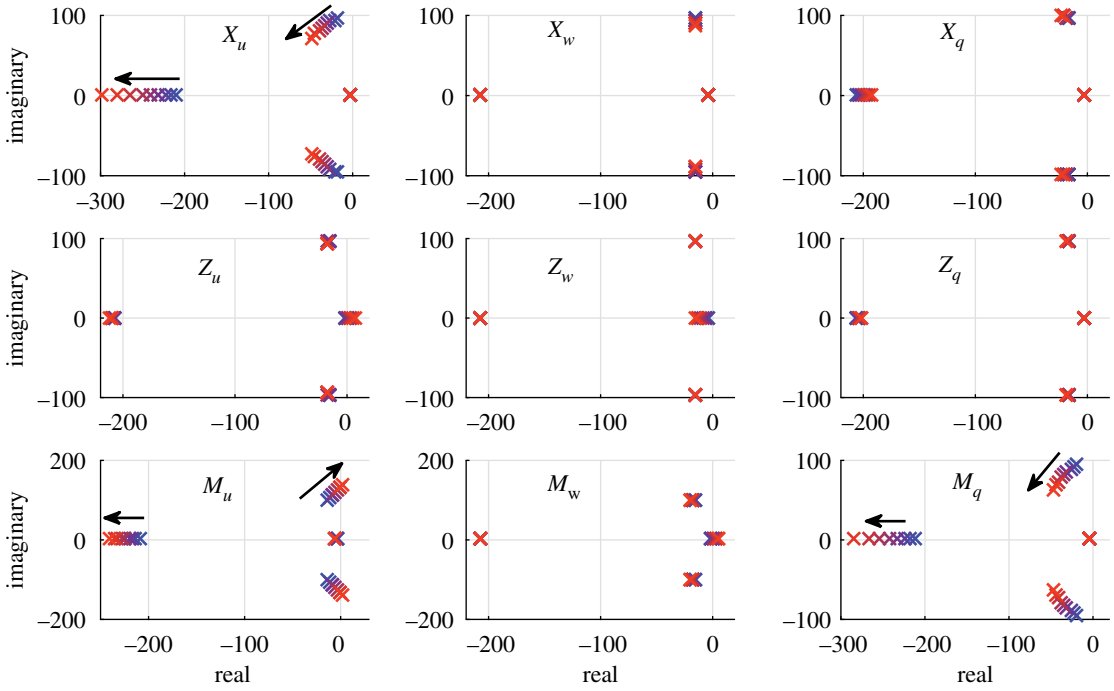

Figure 3. Variation of the open-loop poles with respect to a change in stability derivatives. Poles are plotted for flexible wings with $f/f_1 = 0.41$, while varying each of the nine primary stability derivatives and holding all the rest constant. In each plot, a single stability derivative is varied from its nominal value to a factor 2.5 of its base value. As the stability derivative is increased, the flexible results vary from blue to red. The units of each axis are period^{-1}.

lift produced by the obtained wing motion including the passive pitch angles is similar to those of fruit flies [9]. In hover, the time-averaged lift offsets the weight and time-averaged drag is zero. (iii) The resulting specific power including the aerodynamic and inertial terms is also within the range that is reported for fruit flies [9].

3.2. Hover equilibrium is unstable for rigid wings

The primary reason for the instability of the rigid wing models is the large magnitude of the stability derivative M_u relative to the others [8,12,43]. The derivative M_u is the rate at which an insect tends to pitch up in the presence of a horizontal velocity perturbation. In spite of the various sources of damping that exist in the system, this large pitch rate causes the insect to diverge away from equilibrium, albeit at a rate that ranges from 29 (for hawkmoths) to 114 times (for hover flies) slower than the flapping frequency across insect types [13].

The physical sources of the large speed derivative experienced by a rigid wing extend directly from several of the unique unsteady force production mechanisms. Insects use these low Reynolds number flight mechanisms, i.e. translational lift from delayed stall, rotational lift and wing–wake interaction, to fly using flapping wing motion [1]. Each of these mechanisms destabilizes the hover equilibrium of an insect with rigid wings. The net rearward translational drag force, acting above the body CG, induces nose-up pitch [8]. Also, the stronger rotational lift during stroke reversal from the advancing to retreating strokes causes a larger nose-up pitch moment than in the opposite half-stroke [5,33]. Finally, the wing–wake interaction, where the wing gains momentum from the near-field vortex structures immediately following stroke reversal, creates a fore-to-aft lift imbalance and induces a nose-up tendency under a gust [33].

3.3. Flexible wings stabilize the unstable mode

When wing flexibility is considered, the unstable oscillatory mode becomes stable (figure 1). The least stable mode has now become the slow subsidence mode associated with the heave dynamics, i.e. the vertical motion of the insect. The fast subsidence mode has become much more stable than for the rigid wings.

To assess the collective effect that each individual stability derivative has on the overall system dynamics, we change the values of the stability derivatives individually, while keeping other stability derivatives constant. The resulting variation in the locations of the poles (figure 3) illustrates the sensitivity of the natural response of the insect to each stability derivative [12]. We consider a representative flexible wing system ($f/f_1 = 0.41$).

Only the stability derivatives X_u, M_u and M_q have a notable impact on the system poles. Similar to the dynamics reported for rigid flapping wings [12], increasing the magnitudes of X_u and M_q have a stabilizing influence on the oscillatory mode, which has become stable for flexible wings. By contrast, M_u is destabilizing, as it has been shown to be in rigid wing studies [8,12].

Compared with the stability derivatives reported in the literature for rigid wings, the insects modelled with flexible wings are more sensitive to perturbations (figure 4). The magnitude of some of these stability derivatives are orders of magnitude higher. These stability derivatives are calculated by comparing the dynamics at hover equilibrium and the response under a perturbation. The main difference in the response of a flexible versus a rigid wing is that not only the surrounding unsteady flow changes due to the imposed perturbation but also the structural response adjusts to the perturbation and the changes in the surrounding flow. On the other hand, the wing shape and motion remains the same for the rigid wing and only the surrounding flow changes under a perturbation. This increased sensitivity does not

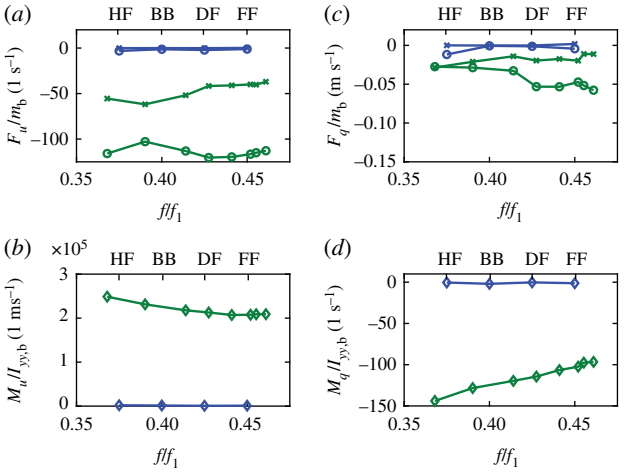

Figure 4. Stability derivatives (*a*) (times) X_u and (open circles) Z_u, (*b*) (open diamonds) M_u, (*c*) (times) X_q and (open circles) Z_q and (*d*) (open diamonds) M_q for the flexible wing with varying f/f_1 (green) and for insect models that assume rigid wings (blue). HF, hover fly [6]; BB, bumblebee [8]; DF, dronefly [6,7]; FF, fruit fly [9].

necessarily mean, however, that the insect is less stable. On the contrary, the increased sensitivity significantly enhances the horizontal velocity damping $-X_u$ and the pitch rate damping $-M_q$ both of which stabilize the insect (figure 3).

The hover equilibrium can be stabilized if the horizontal velocity damping X_u and the pitch rate damping M_q are sufficiently large compared with M_u [12], which is also much greater for the flexible wings. Both X_u and M_q do not need to be greater than M_u in magnitude [12]. For most rigid wing systems, X_u and M_q are too small to stabilize the hover equilibrium [12]. For the considered flexible wing systems, the ability for the wing to deform under perturbation provides the means to sufficiently increase the damping terms X_u and M_q, as described in §§3.3.1. and 3.3.2.

3.3.1. Horizontal velocity damping, X_u

Horizontal velocity damping exists when $X_u < 0$. To explain the increase in horizontal rate damping $-X_u$, we plot the passive pitch angle α_{flex} and the passive pitch rate $\dot{\alpha}_{\text{flex}}$ under perturbation, and the difference between the horizontal accelerations in hover and perturbation $\Delta\dot{u}$ for both a flexible ($f/f_1 = 0.41$) and rigid wing in figure 5. The rigid wing simulation uses the same passive pitch angles that were produced during the hovering case with the flexible wings.

The main mechanism for the differences in $\Delta\dot{u}$ and hence X_u (equation (2.5)) for the two types of wings is that the flexible wing is able to change its response—especially the wing shape—due to the perturbation δu. On the other hand, a rigid wing maintains its shape and moves according to the prescribed kinematics. Since the pitch schedule between the rigid and flexible wing simulations is the same at hover, the pitch and pitch rate for the rigid wing is also the passive pitch angle and its rate for the flexible wing at hover.

The horizontal rate damping $-X_u$ for the flexible wing is enhanced during the portions of the wing stroke labelled a, b, c in figure 5, where the change in horizontal acceleration $\Delta\dot{u}$ is a large negative value. The first occurs from $\tau = 0.2$–0.3

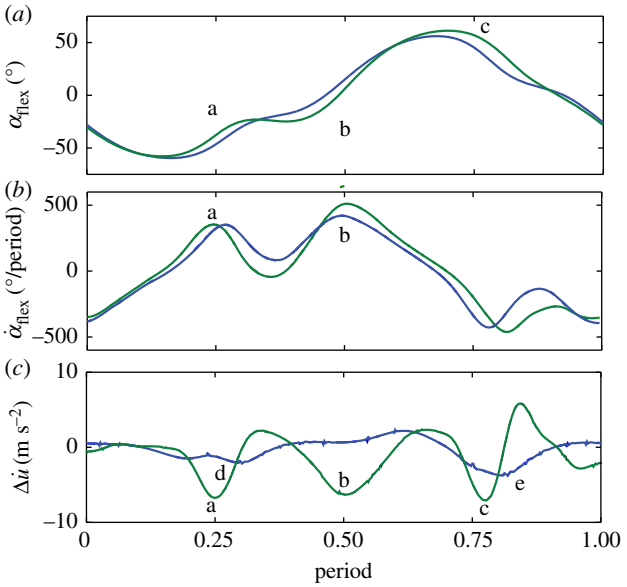

Figure 5. Contributions to the horizontal rate damping, $-X_u$. Flexible wing (green) dynamics at $f/f_1 = 0.41$ with $X_u = -120.3$ are compared with rigid (blue) with $X_u = -19.0$ in response to a perturbation δu in the x_b direction. The pitch schedule is the same for the flexible and rigid wings at hover. Under perturbation, the rigid wing pitch motion remains the same, whereas the wing shape and rates of passive pitch change for the flexible wing. As a consequence, (*a*) the pitch angle α_{flex}, (*b*) pitch rate $\dot{\alpha}_{\text{flex}}$ and (*c*) the change in horizontal acceleration $\Delta\dot{u}$ are different for the flexible and rigid wings under perturbation.

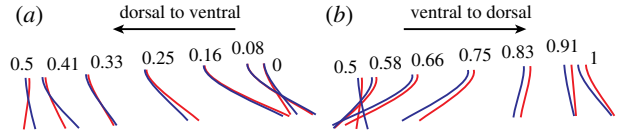

Figure 6. Deformed wing motion for hover (blue) and under a horizontal perturbation (red) for the flexible wing with $f/f_1 = 0.41$. The structural response of the flexible wing in a hover and a gust is not the same, leading to higher horizontal velocity damping.

(station a in figure 5) in the dorsal to ventral stroke, when the horizontal perturbation is opposing the wing motion and the relative velocity of the wing is higher than at hover. This higher relative velocity causes horizontal rate damping ($X_u < 0$) in both the flexible and rigid motion (station d) [5,8]. Clearly, the damping for the flexible wing is larger. The flexible wing shape deformation responds to the horizontal perturbation, reducing its pitch angle (figure 5*a*) and increasing its angle of attack from 44° for the rigid wing to 52° for the flexible wing. Thus, the wing is more vertical, leading to a higher drag and increased damping.

Figure 6 provides the deformed wing position and shape in hover and under perturbation. The wing's response to the perturbation is not simply a matter of the wing being blown back by the higher relative wind in the advancing stroke. Rather, the entire dynamic response changes the time history of deformation throughout the stroke.

There is also a significant horizontal rate damping X_u in the flexible wing case at $\tau = 0.4$–0.6 (station b in figure 5), where no damping exists at all for the rigid wing. This arises primarily due to the larger rotational rate in this

portion of the stroke (figure 5*b*) along with a nearly vertical wing orientation (figure 5*a*). Not only does the wing shape change due to the perturbation, but also its rate. For example, the unperturbed flexible wing has a rotation rate of 369°/period when it is vertical at $\tau = 0.46$, but the perturbed flexible wing has a rotation rate of 492°/period when it is vertical ($\tau = 0.49$), resulting in a larger force oriented in the $-x_b$ direction.

Finally, at $\tau = 0.7$–0.8, the wing is flapping opposite the perturbed body velocity, resulting in a lower relative fluid velocity. The lower dynamic pressure reduces the drag compared with the hover condition for both the flexible (station c of figure 5) and rigid wing (station e of figure 5). However, the flexible wing has lower drag in this portion of the stroke because it has larger passive pitch deformation and therefore lower angle of attack. Additionally, it has a lower rotational velocity than the hover condition, reducing the rotational drag.

Throughout the stroke, the negative contributions in X_u overwhelm the positive contributions, leading to significantly higher horizontal rate damping for the flexible wing than the rigid wing.

3.3.2. Pitch rate damping, M_q

Pitch rate damping exists when $M_q < 0$, which indicates that a nose-up (positive) pitch rate of the body yields a nose-down (negative) moment and pitch acceleration. As $-M_q$ increases, the stability improves. Figure 7 depicts the difference in the pitch acceleration $\Delta\dot{q}$ for the flexible and rigid wings while experiencing a body pitch rate compared with hover. The change in pitch acceleration $\Delta\dot{q}$ directly informs the pitch rate damping M_q. Once again, the trace of flexible wing remains negative for most of the stroke, with significant local peaks of damping at stations a, b and c in figure 7.

The main peak in the pitch rate damping M_q for the flexible wing occurs from $\tau = 0.13$ to 0.42 (station b in figure 7). At the beginning of the stroke (station a), the passive pitch angle due to wing deformation under perturbation is higher than for the hover solution in this region. The larger wing deflection implies that the angle of attack and, hence, drag is lower. Lower drag reduces the nose-up pitch moment about the CG compared with hover, which yields $\Delta\dot{q} < 0$. Also, during station b, the passive pitch angle is lower with the perturbation, producing less lift. At this portion of the stroke, the wing is now in front of the body CG, and less lift produces $\Delta\dot{q} < 0$.

In the second half-stroke, the rigid wing exhibits a stabilizing trend because the direction of the perturbation δq is now opposite. For the flexible wing, the large region of damping from $\tau = 0.65$ to 0.86 (station c) exists largely due to decreased passive pitch angle, leading to higher angles of attack. The more vertical wing orientation creates more drag towards the front of the insect ($-x_b$ direction) in this portion of the stroke. Acting above the body CG, the drag causes a nose-down pitching moment, further contributing to the pitch rate damping.

3.4. Evolution of flight from hover

The locations of the open-loop poles of the flexible flapping wing system suggest that the hover equilibrium is stable.

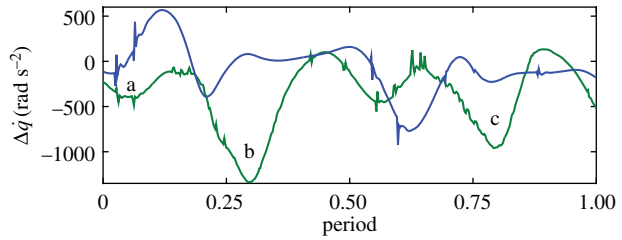

Figure 7. Difference in pitch acceleration between hover and during a q-perturbation $\Delta\dot{q}$ for the flexible (green) at $f/f_1 = 0.41$ and rigid (blue) wings. The values of pitch rate damping are $M_q = -114.4$ for the flexible wing and $M_q = -66.3$ for the rigid wing.

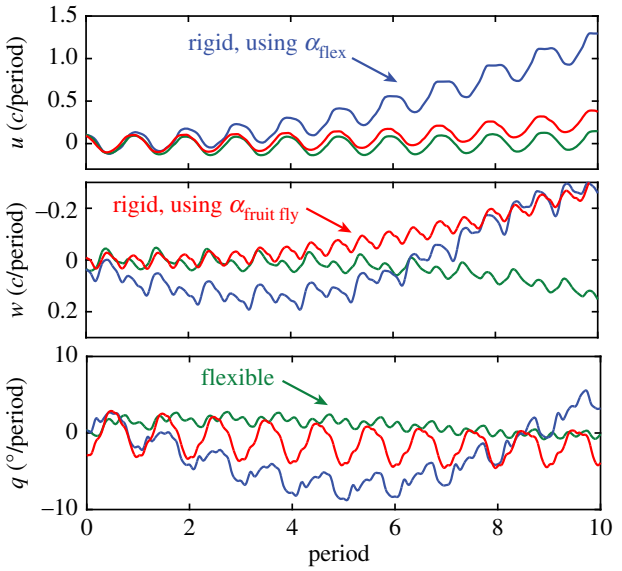

Figure 8. The longitudinal evolution of flight when released from hover for flexible and rigid wings. The rigid wing results consist of a pitch motion from observations of hovering fruit flies [10] (red) and a motion with the pitch schedule based on the flexible wing response (blue). The flexible wing dynamics correspond to $f/f_1 = 0.41$ (green).

However, the stability derivatives were determined by conducting linearization about the equilibrium state of the averaged system dynamics—a common and necessary first step [2,4]. While this technique is powerful in its ability to reveal valuable information about the participation of each degree of freedom in the natural modes of motion, the real system is nonlinear and time-varying. The lift production can be affected by the time-history effects of the vortex dynamics. For example, a persistent downward jet, a nonlinear wing–wake interaction mechanism, can decrease the lift production [49].

To test the hypothesis that wing flexibility passively stabilizes hover, we compare the longitudinal response of the flexible wing to/against two different rigid wing simulations: one with abstracted kinematics and the other with a pitch schedule that matches the flexible wing's passive pitch in figure 8.

Initially, both the flexible and rigid wings are in hover. Even for the unstable response of the rigid wing, the growth in the vertical velocity rate, the highest response, is still less than one chord per period after 10 cycles. The periodic forcing of both wings causes cyclic variations in all

three degrees of freedom. Eventually, both rigid wing systems diverge much more rapidly from the equilibrium than the flexible wing.

The more rapid divergence of the rigid wings further demonstrates that the pitching schedule alone is not enough to stabilize a flapping wing flyer. These results might also explain why the experimentally observed wing pitch kinematics of hovering fruit flies [10] do not appear to confer any stability benefits when simulated with rigid wings. When a biological pitching schedule, which itself results from wing flexibility, is reproduced using a rigid wing simulation, the stability benefits are not seen. The true source of these benefits, i.e. the ability to adjust the wing shape and its dynamics under some perturbation, is not simulated.

4. Concluding remarks

Our stability analysis of the linearized, open-loop flight dynamics model of a flexible flapping wing flyer shows that all eigenvalues have negative real parts. These results suggest that the hover flight of a flapping wing flyer with flexible wings is stable. This is a novel finding as most, if not all, rigid flapping wing studies at fruit fly scales have reported a hover equilibrium with at least one pole with a positive real part. Additionally, we identify that the wing's increased sensitivity to horizontal and pitch perturbations is the physical mechanism for the increased horizontal velocity damping and pitch rate damping and the corresponding improvement in stability. Furthermore, longitudinal simulations in time of flexible wings showed significantly less divergence from the initial condition than rigid wing simulations. Studies in the literature modelled insect wings as being rigid and therefore likely overpredicted their hover instability.

However, these findings are in principle only valid for the considered simplified fruit fly model. Also, this study only considers the effects of chordwise flexibility in a two-dimensional flow velocity field. There are geometric projection differences between a full three-dimensional flapping wing and a two-dimensional plunge motion, particularly when the flapping amplitude is large. These geometric differences might result in minor differences in the resulting longitudinal dynamics and potentially cause differences in the lateral dynamics as well. A real insect wing is three-dimensional with complicated vein patterns and non-uniform anisotropic wing structures. The wing kinematics are also three-dimensional with wing rotation at the wing root. The lateral dynamics are also important, but the associated spanwise flow and lateral forces cannot be accurately modelled without considering more of the three-dimensional fluid dynamics and structural features. Modelling the three-dimensional flexible wings and analysing their effects on the unsteady aerodynamics and six degree-of-freedom flight dynamics and control are very interesting and are left as future study. That said, the primary stabilizing mechanism from wing flexibility may still exist in three-dimensional flapping wing dynamics, particularly because the chordwise flexibility is much more pronounced in insects than the spanwise flexibility.

Recent investigations have demonstrated that flexible flapping wings can enhance lift while reducing power consumption [9,24]. Results from this study suggest that the use of a compliant wing can lead to a novel dynamic benefit that wing flexibility can passively stabilize flight at hover. This does not necessarily imply that insects are truly stable in the open-loop sense—rather, it simply demonstrates that the chordwise wing flexibility has a stabilizing influence on flapping wing flight. Many other morphological parameters can affect insect flight stability including centre-of-gravity location with respect to the wings [4]. Some insect configurations may ultimately prove to remain unstable while others might actually be stable when all of the physics are properly captured. This range of stability would mirror our experience with fixed-wing aircraft, some of which are designed to be inherently stable while others are not. Thus, wing flexibility provides a more stable platform, and flexible wings do not need an active pitching mechanism to achieve a desired pitching motion. It is also possible that the sensing and control system could be reduced in view of the more stable dynamics of flexible wings. Such reductions in weight and complexity are highly attractive to designers because the physical dimensions of FWMAVs are, by definition, extremely small compared with typical air vehicles. Additionally, flexible wings are likely to be made from lighter materials than rigid wings. These combined weight savings might also yield significantly higher payload, range, endurance or agility.

Data accessibility. All numerical data are described in this manuscript. The numerical methodology is described and presented in our previous work [9].

Authors' contributions. C.-k.K. conceived of the study. J.E.B. and C.-k.K. designed the study, developed the mathematical framework required and performed the analysis. J.E.B., M.K.S. and C.-k.K. analysed the model and drafted the manuscript.

Competing interests. We have no competing interests.

Funding. This study is in part supported by NSF CMMI-1761618.

Appendix A. Governing equations

The equation of motion for a flapping wing flyer in three-dimensional space is given as follows:

$$\begin{aligned}
&\left(m_b + \sum_{i=1}^{\#\text{wings}} m_{w,i}\right) {}_b\dot{\mathbf{v}}_b - \sum_{i=1}^{\#\text{wings}} m_{w,i}\, {}_b(\tilde{\mathbf{r}}_{o/\text{cg}}\dot{\boldsymbol{\omega}}_b) \\
&- \sum_{i=1}^{\#\text{wings}} m_{w,i}\left(\underset{w,i\to b}{R}\, {}_w\tilde{\mathbf{r}}_{\text{wg}/o}\, \underset{b\to w,i}{R}\right) {}_b\dot{\boldsymbol{\omega}}_b \\
&= {}_b\mathbf{F}_{\text{Aero},b} + m_b\, {}_b\mathbf{g} + \sum_{i=1}^{\#\text{wings}} ({}_b\mathbf{F}_{\text{Aero},w,i} + m_{w,i}\, {}_b\mathbf{g}) - m_b\, {}_b\tilde{\boldsymbol{\omega}}_b\, {}_b\mathbf{v}_b \\
&- \sum_{i=1}^{\#\text{wings}} m_{w,i}({}_b\tilde{\boldsymbol{\omega}}_b\, {}_b\mathbf{v}_b + {}_b\tilde{\boldsymbol{\omega}}_b\, {}_b\tilde{\boldsymbol{\omega}}_b\, {}_b\mathbf{r}_{o/\text{cg}}) \\
&- \sum_{i=1}^{\#\text{wings}} m_{w,i}\, \underset{w,i\to b}{R}\Big(\underline{{}_w\dot{\mathbf{v}}_{\text{wg}/o} + 2\,{}_w\tilde{\boldsymbol{\omega}}_{ww}\mathbf{v}_{\text{wg}/o}} \\
&\qquad\qquad \underline{- {}_w\tilde{\mathbf{r}}_{\text{wg}/o}\, {}_w\dot{\boldsymbol{\omega}}_{w/b} + {}_w\tilde{\boldsymbol{\omega}}_w\, {}_w\tilde{\boldsymbol{\omega}}_w\, {}_w\mathbf{r}_{\text{wg}/o}}\Big)
\end{aligned} \tag{A 1}$$

$$
\begin{aligned}
&{}_bI_{b,\mathrm{cg}}\,{}_b\dot{\boldsymbol{\omega}}_b + \sum_{i=1}^{\#\mathrm{wings}} \underset{w,i\to b}{R}\,({}_wI_{w,o}\,\underset{b\to w,i}{R}\,{}_b\dot{\boldsymbol{\omega}}_b)_i \\
&+ \sum_{i=1}^{\#\mathrm{wings}} \left(\underset{w,i\to b}{R}\,{}_w\tilde{\mathbf{r}}_{\mathrm{wg}/o}\,\underset{b\to w,i}{R}\,m_w({}_b\dot{\mathbf{v}}_{\mathrm{cg}} - \tilde{\mathbf{r}}_{o/\mathrm{cg}}\,{}_b\dot{\boldsymbol{\omega}}_b)\right)_i \\
&\quad - \sum_{i=1}^{\#\mathrm{wings}} m_{w,i}\,{}_b\tilde{\mathbf{r}}_{o/\mathrm{cg},i}(\underset{w,i\to b}{R}\,{}_w\tilde{\mathbf{r}}_{\mathrm{wg}/o}\,\underset{b\to w,i}{R}\,{}_b\dot{\boldsymbol{\omega}}_b) \\
&+ \sum_{i=1}^{\#\mathrm{wings}} m_{w,i}\,{}_b\tilde{r}_{o/\mathrm{cg},i}({}_b\dot{\mathbf{v}}_{\mathrm{cg}/I} + {}_b\dot{\tilde{\boldsymbol{\omega}}}_b\,{}_b\mathbf{r}_{o/\mathrm{cg}})_i \\
&= M_{\mathrm{Aero,body}} + {}_b\tilde{\mathbf{r}}_{ac,b/\mathrm{cg}}\,{}_bF_{\mathrm{Aero,body}} \\
&\quad + \sum_{i=1}^{\#\mathrm{wings}} \underset{w,i\to b}{R}\,({}_w\mathbf{M}_{\mathrm{Aero},w} + {}_w\tilde{\mathbf{r}}_{ac/o w}\mathbf{F}_{\mathrm{Aero},w} + m_w\,{}_w\tilde{\mathbf{r}}_{\mathrm{wg}/o}\,{}_w\mathbf{g})_i \\
&+ \sum_{i=1}^{\#\mathrm{wings}} {}_b\tilde{\mathbf{r}}_{o/\mathrm{cg},i}\,\underset{w,i\to b}{R}\,({}_wF_{\mathrm{Aero,wing}} + m_w\,{}_w\mathbf{g})_i \\
&\quad - {}_b\tilde{\boldsymbol{\omega}}_b\,{}_bI_{b,\mathrm{cg}}\,{}_b\boldsymbol{\omega}_b \\
&\quad - \sum_{i=1}^{\#\mathrm{wings}} \underset{w,i\to b}{R}\,(\underline{{}_wI_{w,o}\,{}_w\dot{\boldsymbol{\omega}}_{w/b} + {}_w\tilde{\boldsymbol{\omega}}_w\,{}_wI_{w,o}\,{}_w\boldsymbol{\omega}_w}) \\
&\quad - \sum_{i=1}^{\#\mathrm{wings}} \left(\underset{w,i\to b}{R}\,{}_w\tilde{\mathbf{r}}_{\mathrm{wg}/o} m_w[{}_b\tilde{\boldsymbol{\omega}}_b\,{}_bv_{\mathrm{cg}} + {}_b\tilde{\boldsymbol{\omega}}_b\,{}_b\tilde{\boldsymbol{\omega}}_b\,{}_b\mathbf{r}_{o/\mathrm{cg}}]\right) \\
&\quad - \sum_{i=1}^{\#\mathrm{wings}} m_{w,i}\,{}_b\tilde{\mathbf{r}}_{o/\mathrm{cg},i}\,\underset{w,i\to b}{R}\left[\begin{array}{c}-{}_w\tilde{\mathbf{r}}_{\mathrm{wg}/o}\,{}_w\dot{\boldsymbol{\omega}}_{w/b} + {}_w\tilde{\boldsymbol{\omega}}_w\,{}_w\tilde{\boldsymbol{\omega}}_w\,{}_wr_{\mathrm{wg}/o} \\ \underline{\underline{+{}_w\dot{\mathbf{v}}_{\mathrm{wg}/o} + 2{}_w\tilde{\boldsymbol{\omega}}_w\,{}_w\mathbf{v}_{\mathrm{wg}/o}}}\end{array}\right]_i \\
&\quad - \sum_{i=1}^{\#\mathrm{wings}} m_{w,i}\,{}_b\tilde{\mathbf{r}}_{o/\mathrm{cg},i}({}_b\tilde{\boldsymbol{\omega}}_{bb}\mathbf{v}_{\mathrm{cg}} + {}_b\tilde{\boldsymbol{\omega}}_b\,{}_b\tilde{\boldsymbol{\omega}}_b\,{}_b\mathbf{r}_{o/\mathrm{cg}})_i,
\end{aligned}
\tag{A 2}
$$

where $\mathbf{v}$ and $\boldsymbol{\omega}$ denote the velocity and angular rate vector of the subscripted object; $\mathbf{r}_{o/\mathrm{cg}}$ is the position vector from the body CG cg to the wing root o; $\mathbf{r}_{\mathrm{wg}/o}$ is the position vector from the wing root o to the wing CG wg; $\mathbf{g}$ is the acceleration of gravity vector; I_{b} is the inertia tensor about the body CG; $I_{\mathrm{wg},o}$ is the inertial tensor of the wing about the wing root and $\underset{\mathrm{w},i\to\mathrm{b}}{R}$ is the transformation matrix that rotates a vector in the wing frame to the body frame. The leading subscript (w or b) of a vector denotes the reference frame within which the vector is expressed. Other terms follow the same convention and are as follows: $m_{\mathrm{w},i}$ and m_{b} is the mass of the ith wing or body, respectively. An over-dot indicates a local time derivative. The tilde over a vector quantity denotes a cross product.

There are two main differences of the considered equation of motion for flexible wings compared with rigid wing models. In rigid wing studies [6,50], the wing motion is prescribed. In this study, the wing motion is a result of the combination of the body motion, imposed flapping angle and passive pitch angle due to wing deformation. These terms are indicated with single-underlines in equations (A 1 and A 2). Moreover, the double-underlined terms only exist for flexible flapping wing models.

The aerodynamic forces ${}_b\mathbf{F}_{\mathrm{Aero}}$ and moments ${}_b\mathbf{M}_{\mathrm{Aero}}$ produced by the wing are calculated by integrating the pressure and viscous shear stress distribution on the wing that is in dynamic balance between the inertial forces due to the wing and body motion, elastic restoring force from the wing flexibility and aerodynamic forces.

The chordwise flexibility of the wing is modelled with the non-dimensional Euler–Bernoulli beam equation given as follows [31]:

$$
\Pi_0\frac{\partial^2 v^*}{\partial \tau^2} + \Pi_1\Delta^{*2}v^* = F^*, \tag{A 3}
$$

which describes the transverse deflection of the beam v as a function of space and time. The time is normalized by the flapping period $1/f$, i.e. $\tau = ft$, and lengths are normalized by the chord $v^* = v/c$. The effective inertia is the inertia of the wing normalized by the fluid dynamic forces given by $\Pi_0 = \rho^* h_{\mathrm{s}}{}^*(k/\pi)^2$ [31], where ρ^* is the ratio of wing density ρ_{w} to the density of air ρ. The reduced frequency k in hover reduces to a geometric relationship that is governed by the stroke amplitude: $k = \pi fc/U = c/(2Zr_2)$. The reduced frequency for all simulations based on the flapping amplitude required to hover is $k = 0.20$–0.25, which is the same reduced frequency range of fruit flies and other insects [31]. The effective stiffness normalizes the wing stiffness by the fluid dynamic variables and is given by $\Pi_1 = Eh_{\mathrm{s}}{}^*/(12\rho U^2)$ [31].

In equation (A 3), the force $F^* = F/(c\rho U^2)$ is the non-dimensional transverse component of the aerodynamic forces F per unit length. This force is determined from the pressure distribution based on the solutions to the unsteady, viscous, incompressible, two-dimensional Navier–Stokes equations:

$$
\left.\begin{aligned}
\nabla^*\cdot\mathbf{V}^* &= 0 \\
\frac{k}{\pi}\frac{\partial \mathbf{V}^*}{\partial \tau} + (\mathbf{V}^*\cdot\nabla^*)\mathbf{V}^* &= -\nabla^* p^* + \frac{1}{\mathrm{Re}}\Delta^*\mathbf{V}^*,
\end{aligned}\right\} \tag{A 4}
$$

where the velocity field $\mathbf{V}$ is normalized with the reference velocity U, or $\mathbf{V}^* = \mathbf{V}/U$. Lengths are again normalized by c, and pressure is normalized per $p^* = p/\rho U^2$. The Reynolds number is defined as $\mathrm{Re} = Uc/\nu$, where the kinematic viscosity is for air $\nu = 1.7073\times10^{-5}\ \mathrm{m^2\,s^{-1}}$. At the considered reduced frequency of $k = 0.20$–0.25, the flow is unsteady, suggesting that only the unsteady Navier–Stokes equations can resolve the true nature of the fluid dynamics. Full details of the computational methodology are described in our previous work [9].

References

1. Dickinson MH, Lehmann F-O, Sane SP. 1999 Wing rotation and the aerodynamic basis of insect flight. *Science* **284**, 1954–1960. (doi:10.1126/science.284.5422.1954)
2. Sun M. 2014 Insect flight dynamics: stability and control. *Rev. Mod. Phys.* **86**, 615–646. (doi:10.1103/RevModPhys.86.615)
3. Orlowski CT, Girard AR. 2012 Dynamics, stability, and control analyses of flapping wing micro-air vehicles. *Prog. Aerosp. Sci.* **51**, 18–30. (doi:10.1016/j.paerosci.2012.01.001)
4. Taha HE, Hajj MR, Nayfeh AH. 2012 Flight dynamics and control of flapping-wing MAVs: a review. *Nonlinear Dyn.* **70**, 907–939. (doi:10.1007/s11071-012-0529-5)
5. Cheng B, Deng X. 2011 Translational and rotational damping of flapping flight and its dynamics and stability at hovering. *IEEE Trans. Robot.* **27**, 849–864. (doi:10.1109/TRO.2011.2156170)
6. Sun M, Wang JK, Xiong Y. 2007 Dynamic flight stability of hovering insects. *Acta Mech. Sin.* **23**, 231–246. (doi:10.1007/s10409-007-0068-3)

7. Zhang Y-L, Sun M. 2010 Dynamic flight stability of hovering model insects: theory versus simulation using equations of motion coupled with Navier–Stokes equations. *Acta Mech. Sin.* **26**, 509–520. (doi:10.1007/s10409-010-0360-5)
8. Sun M, Xiong Y. 2005 Dynamic flight stability of a hovering bumblebee. *J. Exp. Biol.* **208**, 447–459. (doi:10.1242/jeb.01407)
9. Bluman JE, Kang C. 2017 Achieving hover equilibrium in free flight with a flexible flapping wing. *J. Fluids Struct.* **75**, 117–139. (doi:10.1016/j.jfluidstructs.2017.08.011)
10. Fry SN, Sayaman R, Dickinson MH. 2005 The aerodynamics of hovering flight in *Drosophila*. *J. Exp. Biol.* **208**, 2303–2318. (doi:10.1242/jeb.01612)
11. Shyy W, Kang C, Chirarattananon P, Ravi S, Liu H. 2016 Aerodynamics, sensing and control of insect-scale flapping-wing flight. *Proc. R. Soc. A Math. Phys. Eng. Sci.* **472**, 20150712. (doi:10.1098/rspa.2015.0712)
12. Taha HE, Hajj MR, Nayfeh AH. 2014 Longitudinal flight dynamics of hovering MAVs/insects. *J. Guidance Control Dyn.* **37**, 970–979. (doi:10.2514/1.62323)
13. Taha HE, Tahmasian S, Woolsey CA, Nayfeh AH, Hajj MRMR. 2015 The need for higher-order averaging in the stability analysis of hovering, flapping-wing flight. *Bioinspir. Biomim.* **10**, 16002. (doi:10.1088/1748-3190/10/1/016002)
14. Faruque I, Humbert JS. 2010 Dipteran insect flight dynamics. Part 1: longitudinal motion about hover. *J. Theor. Biol.* **264**, 538–552. (doi:10.1016/j.jtbi.2010.02.018)
15. Liang B, Sun M. 2013 Nonlinear flight dynamics and stability of hovering model insects. *J. R. Soc. Interf.* **10**, 20130269. (doi:10.1098/rsif.2013.0269)
16. Wu JH, Sun M. 2012 Floquet stability analysis of the longitudinal dynamics of two hovering model insects. *J. R. Soc. Interf.* **9**, 2033–2046. (doi:10.1098/rsif.2012.0072)
17. Mou X, Sun M. 2012 Dynamic flight stability of a model hoverfly in inclined-stroke-plane hovering. *J. Bionic Eng.* **9**, 294–303. (doi:10.1016/S1672-6529(11)60123-6)
18. Mountcastle AM, Combes SA. 2013 Wing flexibility enhances load-lifting capacity in bumblebees. *Proc. R. Soc. B* **280**, 20130531. (doi:10.1098/rspb.2013.0531)
19. Combes SA, Daniel TL. 2003 Flexural stiffness in insect wings I. Scaling and the influence of wing venation. *J. Exp. Biol.* **206**, 2979–2987. (doi:10.1242/jeb.00523)
20. Combes SA, Daniel TL. 2003 Flexural stiffness in insect wings II. Spatial distribution and dynamic wing bending. *J. Exp. Biol.* **206**, 2989–2997. (doi:10.1242/jeb.00524)
21. Ennos ARR. 1988 The inertial cause of wing rotation in Diptera. *J. Exp. Biol.* **140**, 161–169.
22. Ramananarivo S, Godoy-Diana R, Thiria B. 2011 Rather than resonance, flapping wing flyers may play on aerodynamics to improve performance. *Proc. Natl Acad. Sci. USA* **108**, 5964–5969. (doi:10.1073/pnas.1017910108)
23. Eldredge JD, Toomey J, Medina A. 2010 On the roles of chord-wise flexibility in a flapping wing with hovering kinematics. *J. Fluid Mech.* **659**, 94–115. (doi:10.1017/S0022112010002363)
24. Kang C-K, Shyy W. 2013 Scaling law and enhancement of lift generation of an insect-size hovering flexible wing. *J. R. Soc. Interf.* **10**, 20130361. (doi:10.1098/rsif.2013.0361)
25. Berman GJ, Wang ZJ. 2007 Energy-minimizing kinematics in hovering insect flight. *J. Fluid Mech.* **582**, 153–168. (doi:10.1017/S0022112007006209)
26. Badrya C, Sridharan A, Baeder JD, Kroninger CM. 2017 Multi-fidelity coupled trim analysis of a flapping-wing micro air vehicle flight. *J. Aircraft* **54**, 1614–1630. (doi:10.2514/1.C034236)
27. Shyy W, Aono H, Kang C, Liu H. 2013 *An introduction to flapping wing aerodynamics*. New York, NY: Cambridge University Press.
28. Shyy W, Aono H, Chimakurthi SKK, Trizila P, Kang C, Cesnik CESES, Liu H. 2010 Recent progress in flapping wing aerodynamics and aeroelasticity. *Prog. Aerosp. Sci.* **46**, 284–327. (doi:10.1016/j.paerosci.2010.01.001)
29. Sane SP. 2003 The aerodynamics of insect flight. *J. Exp. Biol.* **206**, 4191–4208. (doi:10.1242/jeb.00663)
30. de Boer A, van der Schoot MSS, Bijl H. 2007 Mesh deformation based on radial basis function interpolation. *Comput. Struct.* **85**, 784–795. (doi:10.1016/j.compstruc.2007.01.013)
31. Kang C-K, Aono H, Cesnik CES, Shyy W. 2011 Effects of flexibility on the aerodynamic performance of flapping wings. *J. Fluid Mech.* **689**, 32–74. (doi:10.1017/jfm.2011.428)
32. Chimakurthi SK, Tang J, Palacios R, Cesnik CES, Shyy WS. 2009 Computational aeroelasticity framework for analyzing flapping wing micro air vehicles. *AIAA J.* **47**, 1865–1878. (doi:10.2514/1.38845)
33. Bluman JE, Kang C-K. 2017 Wing–wake interaction destabilizes hover equilibrium of a flapping insect-scale wing. *Bioinspir. Biomim.* **12**, 46004. (doi:10.1088/1748-3190/aa7085)
34. Ellington CP. 1984 The aerodynamics of hovering insect flight. IV. Aeorodynamic mechanisms. *Phil. Trans. R. Soc. Lond. B.* **305**, 79–113. (doi:10.1098/rstb.1984.0052)
35. Lua KB, Lim TT, Yeo KS. 2014 Scaling of aerodynamic forces of three-dimensional flapping wings. *AIAA Journal* **52**, 1–7. (doi:10.2514/1.J052730)
36. Birch JM, Dickinson MH. 2001 Spanwise flow and the attachment of the leading-edge vortex on insect wings. *Nature* **412**, 729–733. (doi:10.1038/35089071)
37. Shyy W, Trizila P, Kang C-K, Aono H. 2009 Can tip vortices enhance lift of a flapping wing? *AIAA J.* **47**, 289–293. (doi:10.2514/1.41732)
38. Lentink D, Dickinson MH. 2009 Rotational accelerations stabilize leading edge vortices on revolving fly wings. *J. Exp. Biol.* **212**, 2705–2719. (doi:10.1242/jeb.022269)
39. Shyy W, Liu H. 2007 Flapping wings and aerodynamic lift: the role of leading-edge vortices. *AIAA J.* **45**, 2817–2819. (doi:10.2514/1.33205)
40. Wang ZJ, Birch JM, Dickinson MH. 2004 Unsteady forces and flows in low Reynolds number hovering flight: two-dimensional computations vs robotic wing experiments. *J. Exp. Biol.* **207**, 449–460. (doi:10.1242/jeb.00739)
41. Wang ZJ. 2005 Dissecting insect flight. *Annu. Rev. Fluid Mech.* **37**, 183–210. (doi:10.1146/annurev.fluid.36.050802.121940)
42. Alben S, Shelley M. 2005 Coherent locomotion as an attracting state for a free flapping body. *Proc. Natl Acad. Sci. USA* **102**, 11 163–11 166. (doi:10.1073/pnas.0505064102)
43. Cheng B, Deng X, Hedrick TL. 2011 The mechanics and control of pitching manoeuvres in a freely flying hawkmoth (*Manduca sexta*). *J. Exp. Biol.* **214**, 4092–4106. (doi:10.1242/jeb.062760)
44. Lehmann F-O, Dickinson MH. 1997 The changes in power requirements and muscle efficiency during elevated force production in the fruit fly *Drosophila melanogaster*. *J. Exp. Biol.* **200**, 1133–1143.
45. Lehmann F-O, Gorb S, Nasir N, Schutzner P, Schützner P. 2011 Elastic deformation and energy loss of flapping fly wings. *J. Exp. Biol.* **214**, 2949–2961. (doi:10.1242/jeb.045351)
46. Sunada S, Zeng L, Kawachi K. 1998 The relationship between dragonfly wing structure and torsional deformation. *J. Theor. Biol.* **193**, 39–45. (doi:10.1006/jtbi.1998.0678)
47. Sridhar MK, Kang C. 2015 Aerodynamic performance of two-dimensional, chordwise flexible flapping wings at fruit fly scale in hover flight. *Bioinspir. Biomim.* **10**, 36007. (doi:10.1088/1748-3190/10/3/036007)
48. Bergou AJ, Xu S, Wang ZJ. 2007 Passive wing pitch reversal in insect flight. *J. Fluid Mech.* **591**, 321–337. (doi:10.1017/S0022112007008440)
49. Trizila P, Kang C, Aono H, Shyy W, Visbal M. 2011 Low-Reynolds-number aerodynamics of a flapping rigid flat plate. *AIAA J.* **49**, 806–823. (doi:10.2514/1.J050827)
50. Wu JH, Zhang Y-LL, Sun M. 2009 Hovering of model insects: simulation by coupling equations of motion with Navier–Stokes equations. *J. Exp. Biol.* **212**, 3313–3329. (doi:10.1242/jeb.030494)